Available online at www.sciencedirect.com

SciVerse ScienceDirect

Ceramics International 39 (2013) 6647–6655

CERAMICS INTERNATIONAL

www.elsevier.com/locate/ceramint

Solvothermal synthesis of SnO_2/graphene nanocomposites for supercapacitor application

S.P. Lim[a], N.M. Huang[a,*], H.N. Lim[b,c,**]

[a]Low Dimensional Materials Research Centre, Faculty of Science, Department of Physics, University of Malaya, 50603 Kuala Lumpur, Malaysia
[b]Department of Chemistry, Faculty of Science, Universiti Putra Malaysia, 43400 UPM Serdang, Selangor, Malaysia
[c]Functional Device Laboratory, Institute of Advanced Technology, Universiti Putra Malaysia, 43400 UPM Serdang, Selangor, Malaysia

Received 26 October 2012; received in revised form 14 January 2013; accepted 22 January 2013
Available online 13 February 2013

Abstract

A facile solvent-based synthesis route based on the oxidation–reduction reaction between graphene oxide (GO) and $SnCl_2 \cdot 2H_2O$ has been developed to synthesize SnO_2/graphene (SnO_2/G) nanocomposites. The reduction of GO and the in situ formation of SnO_2 nanoparticles were achieved in one step. Characterization by X-ray diffraction (XRD), ultraviolet-visible (UV–vis) absorption spectroscopy, Raman spectroscopy, and field emission scanning electron microscopy (FESEM) confirmed the feasibility of using the solvothermally treated reaction system to simultaneously reduce GO and form SnO_2 nanoparticles with an average particle size of 10 nm. The electrochemical performance of SnO_2/graphene showed an excellent specific capacitance of 363.3 F/g, which was five-fold higher than that of the as-synthesized graphene (68.4 F/g). The contributing factors were the synergistic effects of the excellent conductivity of graphene and the nanosized SnO_2 particles.

Keywords: B. Nanocomposites; E. Capacitors; Graphene; Tin oxide

1. Introduction

In the enormous effort to achieve energy sustainability, supercapacitors, which are also known as ultracapacitors or electrochemical supercapacitors, are devices that have received extensive attention due to their superior characteristics, including their prolonged life cycle [1,2], higher power density [3], and higher energy density [4], and they are unmatched by any other electrical energy storage devices such as faradic batteries, electrostatic capacitors, electrolytic capacitors, and ceramic capacitors [5]. According to the mechanism of charge storage, supercapacitors can be classified as (i) electrochemical double-layer capacitors (EDLCs), which are based on electrostatic charge diffusion and accumulation at the electrode/electrolyte interface, and (ii) pseudocapacitors, which are dominated by faradic reactions on electrode materials [6,7].

For EDLCs, carbon-based materials are commonly used as electrodes due to their outstanding long-term electrochemical stability as a result of high electrical conductivity and extraordinary chemical stability [8]. Therefore, carbon-based materials such as activated carbon [9], xerogels [10], carbon nanotubes [11], mesoporous carbon [12], and carbide-derived carbons [13] have been investigated for use as electrodes in EDLCs. However, the limited charge accumulation in the electrical double layer restricts the specific capacitance of EDLCs to a range of relatively small values between 90 and 250 F/g [14]. Meanwhile, pseudocapacitors based on metal oxides such as RuO_2 [15–17], NiO [17,18], CoOx [19], and MnO_2 [20,21] or conducting polymers including polypyrrole [22] and polyaniline [23,24] usually show less cycling stability than EDLCs but have high specific capacitance values.

Recently, graphene, a novel and unique EDLC-based carbon material with a one-atom thick layer, has been used as a supercapacitor electrode material due to its high surface area, excellent stability, and good conductivity [25–28].

*Corresponding author. Tel.: +60 12 2091008.
**Corresponding author at: Department of Chemistry, Faculty of Science, Universiti Putra Malaysia, 43400 UPM Serdang, Selangor, Malaysia.
E-mail addresses: huangnayming@um.edu.my (N.M. Huang), janet_limhn@science.upm.edu.my (H.N. Lim).

0272-8842/$ - see front matter © 2013 Elsevier Ltd and Techna Group S.r.l. All rights reserved.
http://dx.doi.org/10.1016/j.ceramint.2013.01.102

To effectively overcome the shortage of low specific capacitance, two-dimensional (2D) structured graphene has been hybridized with pseudocapacitors for the preparation of supercapacitors [29–33]. Tin oxide (SnO_2) is an n-type semiconductor with a wide band gap of 3.6 eV [34]. This metal oxide has received enormous attention due to its unique electrical and optical properties, all of which lead to multiple potential applications. It has a wide range of applications in optoelectronic devices, dye-based solar cells, catalysts, gas sensors, electrochromic devices, and electrode materials [35–38].

Wang and co-workers reported on microwave-assisted one-pot synthesis of SnO_2/graphene, which gave rise to the specific capacitance of 99.7 F/g [29]. Li et al. prepared SnO_2/graphene using a one-pot synthesis approach, which showed a specific capacitance of 34.6 F/g [39]. Based on these findings, more investigations can be done to improve the specific capacitance of nanocomposites to meet the criteria for excellent supercapacitors.

In this report, SnO_2/graphene nanocomposite hydrogel was synthesized using a solvothermal processing route for the first time. This one-pot synthesis strategy is facile and does not require any reducing or oxidizing agent. The in situ growth of SnO_2 led to uniformly decorated nanoparticles on the surface of graphene. The SnO_2/graphene nanocomposite possessed a pronounced enhancement of the electrochemical properties, allowing the nanocomposite to be used as a supercapacitor.

2. Experimental

2.1. Materials

Graphite flakes were purchased from Ashbury Inc. (NJ, US). Sulfuric acid (H_2SO_4, 95–98%), phosphoric acid (H_3PO_4, 85%), potassium permanganate ($KMnO_4$, 99.9%), and hydrogen peroxide (H_2O_2, 30%) were purchased from Merck. Hydrogen chloride (HCl, 37%) was purchased from Sigma-Aldrich. Tin (II) chloride dihydrate ($SnCl_2 \cdot 2H_2O$, 98%) and absolute ethanol were purchased from Merck and HmbG Chemicals, respectively. Distilled water was used throughout the sample preparation.

2.2. Synthesis of graphene oxide

Graphene oxide (GO) was synthesized using a simplified Hummer's method [40]. Graphite flakes (3 g), H_2SO_4 (360 ml), H_3PO_4 (40 ml), and $KMnO_4$ (18 g) were mixed using a magnetic stirrer at room temperature. The mixture was stirred for three days to achieve complete oxidation of the graphite. The color of the mixture changed from dark purplish green to dark brown. H_2O_2 solution was added to stop the oxidation process and the color of the mixture changed to bright yellow, indicating a high oxidation level of graphite oxide. The formed graphite oxide was washed three times with 1 M of HCl aqueous solution and repeatedly – at least six times – with distilled water to achieve a pH of 4–5. The washing process was carried out using a simple decantation of supernatant via the centrifugation technique. During the process of washing with distilled water, the graphite oxide experienced exfoliation, which resulted in the thickening of the GO solution and finally the formation of the GO gel. The concentration of the GO gel obtained was determined.

2.3. Solvothermal synthesis of SnO_2/graphene nanocomposite

GO was dispersed in absolute ethanol to achieve a concentration of 1 mg/ml of GO and was stirred for 30 min until a homogeneous mixture was obtained. Then, 5 mM of $SnCl_2 \cdot 2H_2O$ was added and the mixture was stirred continuously for another 30 min. The resultant mixture was then transferred to a Teflon-lined autoclave and kept in the oven at 180 °C for 24 h. After the autoclave cooled down, the nanocomposite hydrogel was separated and washed with distilled water and ethanol several times by centrifugation. Finally, the product was dried in an oven at 60 °C and was denoted as SnO_2/G. The same procedure was carried out without the presence of $SnCl_2 \cdot 2H_2O$ and the graphene hydrogel was labeled as HGO.

2.4. Characterization

The crystalline phase of the samples was determined by XRD (D5000, Siemens) using copper Kα radiation (λ = 1.5418 Å) at a scan rate of $0.02^{\circ}s^{-1}$. The morphology of SnO_2/graphene was examined by FESEM (FEI Nova NanoSEM 400 operated at 10.0 kV) and high resolution TEM (JEOL JEM-2100 F). Optical absorption properties over the spectral region of 190–900 nm were assessed using a UV–vis spectrophotometer (Thermoscientific Evolution 300). Raman spectra were collected using a Renishaw 2000 system with an argon ion laser of 514.5 nm.

2.5. Cyclic voltammetry

A Model VersaSTAT 3 electrochemical analyzer from Princeton Applied Research was used for the electrochemical characterization. It was equipped with an electrochemical cell consisting of three electrodes: a glassy carbon electrode (GCE, 3 mm in diameter) as the working electrode, Ag/AgCl (in 3 M of NaCl) as the reference electrode, and a platinum wire as the counter electrode. The potential was scanned from 0 to 1.0 V and the scan rate was varied from 10 to 100 mV/s in 1.0 M Na_2SO_4. The galvanostatic charge/discharge curves of HGO and SnO_2/G modified electrodes at a constant current density of 1.0 A/g and in the potential range between 0 and 1 V

Before modification, bare GCE was polished to a mirror-like appearance with alumina slurry on micro-cloth pads, rinsed thoroughly with distilled water for each step of polishing, and then washed excessively with distilled water and absolute ethanol. To prepare SnO_2/G-modified GCE,

an aliquot of 3 μl of 2.0 mg/ml SnO_2/G aqueous solution was coated on the clean GCE with a microsyringe and dried in air before use. The same procedure was repeated for HGO-modified GCE.

3. Results and discussion

In this work, we adopted a convenient in situ chemical synthesis route to fabricate SnO_2 nanoparticles decorated on graphene. For a control experiment and to study the feasibility of the solvothermal method for the reduction of GO to graphene, the mixture was also prepared without the tin precursor. The reduction of GO was examined using UV–vis absorption spectroscopy and the result is shown in Fig. 1. The UV–vis absorption peak for GO is at 228 nm with a shoulder at around 300 nm. The peak at 228 nm is assigned to the $\pi \rightarrow \pi^*$ transitions of the aromatic C–C bonds while the shoulder at 300 nm is due to the $n \rightarrow \pi^*$ transitions of the C=O bonds [41]. However, the peak at 228 nm right-shifted to 255 nm after the solvothermal treatment (HGO), indicating the partial restoration of the π conjugation network in HGO [42]. The shift of the peak position provides evidence for the reduction of surface functional groups on the GO sheets during the solvothermal procedure. The missing 228 nm peak and the appearance of the 255 nm peak for SnO_2/G signify that GO had been reduced to graphene.

To further evaluate the formation of SnO_2/G nanocomposite, Raman spectroscopy was performed on GO, HGO, and SnO_2/G and the profiles are presented in Fig. 2. The peak at around 1344 cm^{-1} (D band) is related to the defects and disorder in the hexagonal lattice, while the 1592 cm^{-1} peak (G band) is due to the vibration of sp^2-bonded carbon atoms in a 2D hexagonal lattice [42,43]. The intensity ratio of the D band to the G band (I_D/I_G) generally reflects the degree of graphitization of carbonaceous materials and the defect density [16].The calculated I_D/I_G ratios are 0.98, 0.82, and 1.00 for GO, HGO, and SnO_2/G, respectively. The I_D/I_G ratio of HGO is lower than that of GO, indicating that the average size of the sp^2 domains of the solvothermally prepared HGO is relatively large [44]. The relatively high I_D/I_G ratio for GO is contributed by the presence of oxide functional groups on the basal planes and edges of the sheets and the exfoliation of GO [45]. However, the I_D/I_G ratio for SnO_2/G is the highest, which suggests a decrease in the average size of the sp^2 domains. This increment of the I_D/I_G ratio is due to the presence of SnO_2 nanoparticles on the graphene sheets. In the SnO_2/G curve, two new peaks appear at 415 and 630 cm^{-1}, which correspond to the E_g and A_{1g} vibration modes of SnO_2, respectively [46].

The XRD pattern obtained for SnO_2/G is shown in Fig. 3, together with those of the as-prepared GO, HGO, and SnO_2. The diffraction peak for GO at 9.8° (Fig. 3a) disappeared in the HGO pattern (Fig. 3b), indicating that GO had been reduced to graphene. The diffraction peaks of SnO_2 (Fig. 3c) and SnO_2/G (Fig. 3d) at around 26.6°, 33.8°, 51.8°, and 65.94° agree well with the rutile phase of SnO_2 with tetragonal structure, which is in accordance with the reference pattern JCPDS 41-1445. The diffraction peaks for both SnO_2 and SnO_2/G are broad, indicating

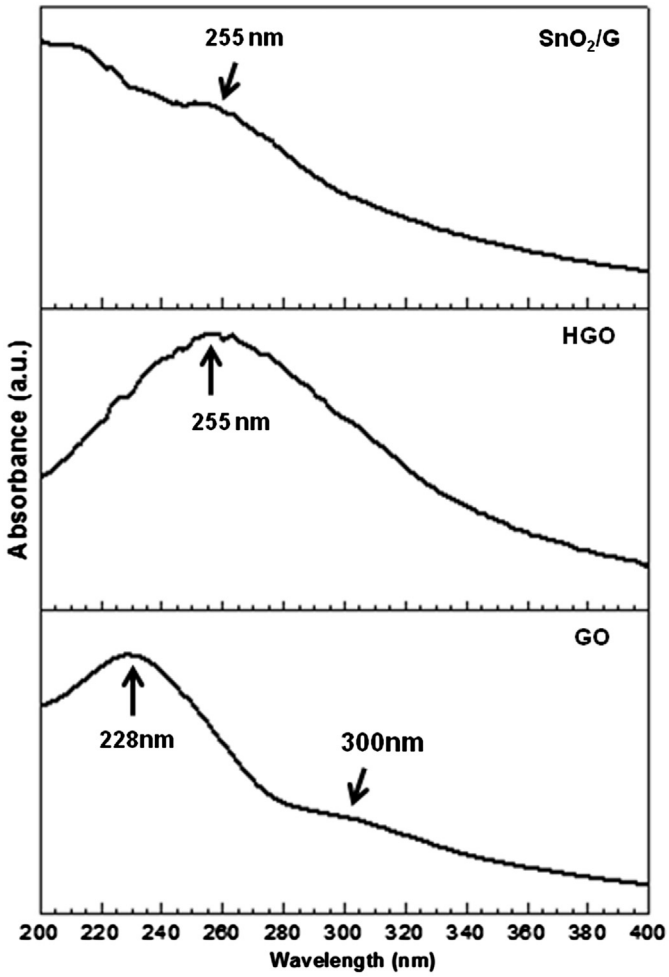

Fig. 1. UV–vis spectra for GO, HGO and SnO_2/G.

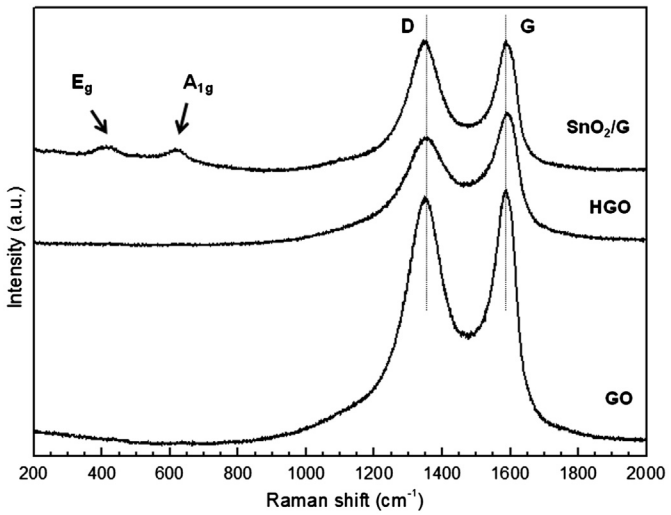

Fig. 2. Raman spectra for GO, HGO and SnO_2/G.

that the SnO_2 particles are nanosized [47]. However, there is a broad impurity peak at 13.4° detected for HGO, SnO_2/G, and SnO_2, which was suspected to be due to the contribution from the XRD sample holder made of Perspex material. Verification of the peak was done by scanning the sample holder (Perspex material) without the sample (Fig. 3e), and a diffraction peak was found at 13.4°. The peak at 13.4° was absent for the GO sample as it was deposited on the glass substrate and not Perspex.

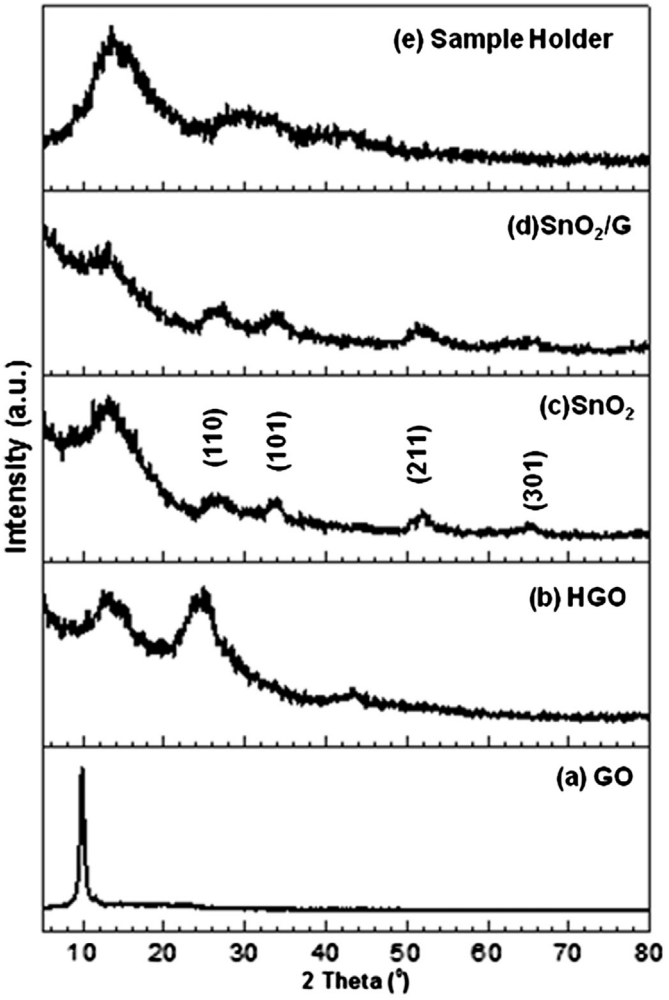

Fig. 3. X-ray diffraction patterns of (a) GO, (b) HGO, (c) SnO_2 (d) SnO_2/G, and (e) sample holder (Perspex material).

The physical appearance of the SnO_2/G nanocomposite after solvothermal treatment is shown in Fig. 4. The dark brown solution (Fig. 4a), comprising GO and Sn^{2+}, was converted to a black cylinder-shaped monolith by the supercritical treatment. The density of the matrix is lower than that of water, enabling it to float in water (Fig. 4b).

The microscopic morphology of the as-prepared samples was studied using FESEM. Fig. 5(a) shows the image of the HGO, which appears creased and layered. Fig. 5(b) shows the image of the SnO_2 nanoparticles prepared using the solvothermal method and having an average size of 95 nm. The overview of the SnO_2/G nanocomposite is illustrated in Fig. 5(c) and is similar to our previous work on graphene hydrogel [48]. The sample is well defined, and the interlinked three-dimensional (3D) graphene sheets, which formed a porous network, resemble a loose sponge-like structure. The hydrothermal condition resulted in overlapping and coalescence to form cross-links, which gave rise to the framework of the graphene hydrogel. Moreover, the large conjugated basal planes make the graphene sheets stiff and able to form a stable network [49]. The images of SnO_2/G at different concentrations of 25 mM, 5 mM, and 2.5 mM are shown in Fig. 5(d–f) respectively. At a high concentration of 25 mM (Fig. 5d), aggregations are observed on the surface of the nanocomposite, whilst at a low concentration of 2.5 mM (Fig. 5f), SnO_2 matter is not distinctive. At 5 mM of Sn^{2+}, SnO_2 nanoparticles are uniformly distributed on the graphene nanosheets (Fig. 5e). The average size of the SnO_2 nanoparticles in the nanocomposite prepared with 5 mM of Sn^{2+} is 10 nm, which is approximately ten times smaller than the as-synthesized SnO_2 nanoparticles. Graphene acted as a support for SnO_2 nanoparticles, thus preventing the aggregation of nanoparticles, unlike the lone SnO_2 nanoparticles that clump together. To determine the

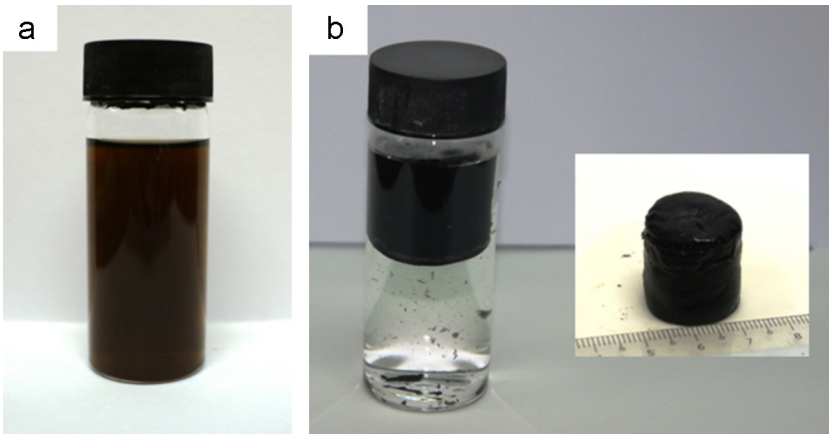

Fig. 4. Physical appearance of (a) GO and Sn^{2+} solution, and (b) SnO_2/G after solvothermal treatment.

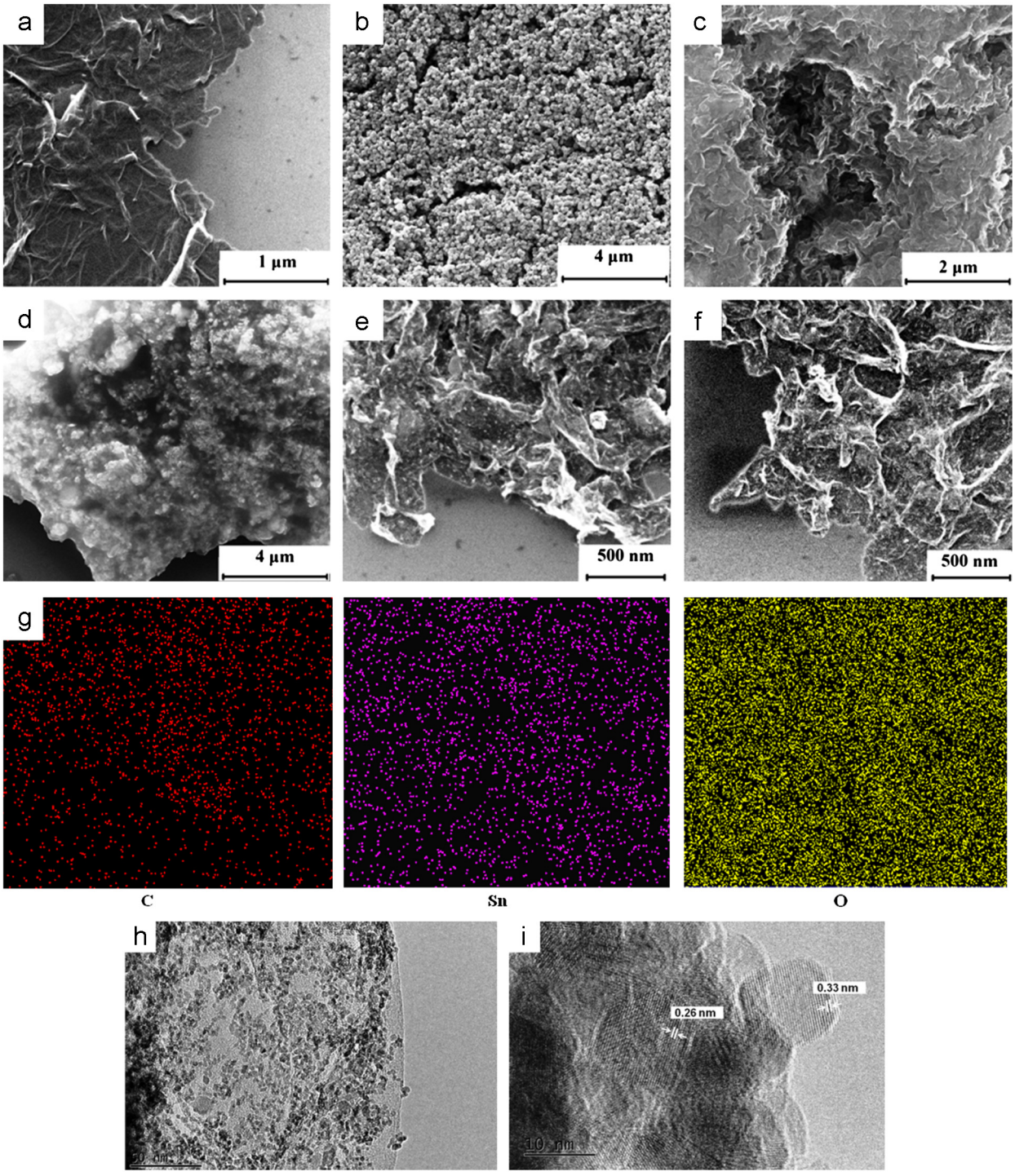

Fig. 5. FESEM images of (a) HGO, (b) SnO_2 nanoparticles (c) low magnification of SnO_2/G nanocomposite, high magnification of SnO_2/G at 25 mM (d), 5 mM (e) and 2.5 mM (f) Sn^{2+}, (g) elemental mapping of SnO_2/G prepared at 2.5 mM Sn^{2+},(h) low magnification HRTEM of SnO_2/G and (i) low magnification HRTEM of SnO_2/G.

presence of SnO_2 on graphene sheets, elemental mapping of SnO_2/G was also performed, as shown in Fig. 5g. The areas of bright contrast correlate with the C, Sn, and O signal maps.

Further HRTEM observation (Fig. 5h and i) reveals that the SnO_2 nanoparticles have a good crystalline structure and an average size of 10 nm and are distributed homogenously on the graphene surface. The HRTEM samples were sonicated for 10 min prior to investigation; thus, it is evident that the bonding between the SnO_2 and graphene is very strong. Some nanoparticles show clear lattice fringes. The lattice spacings of 0.33 nm and 0.26 nm

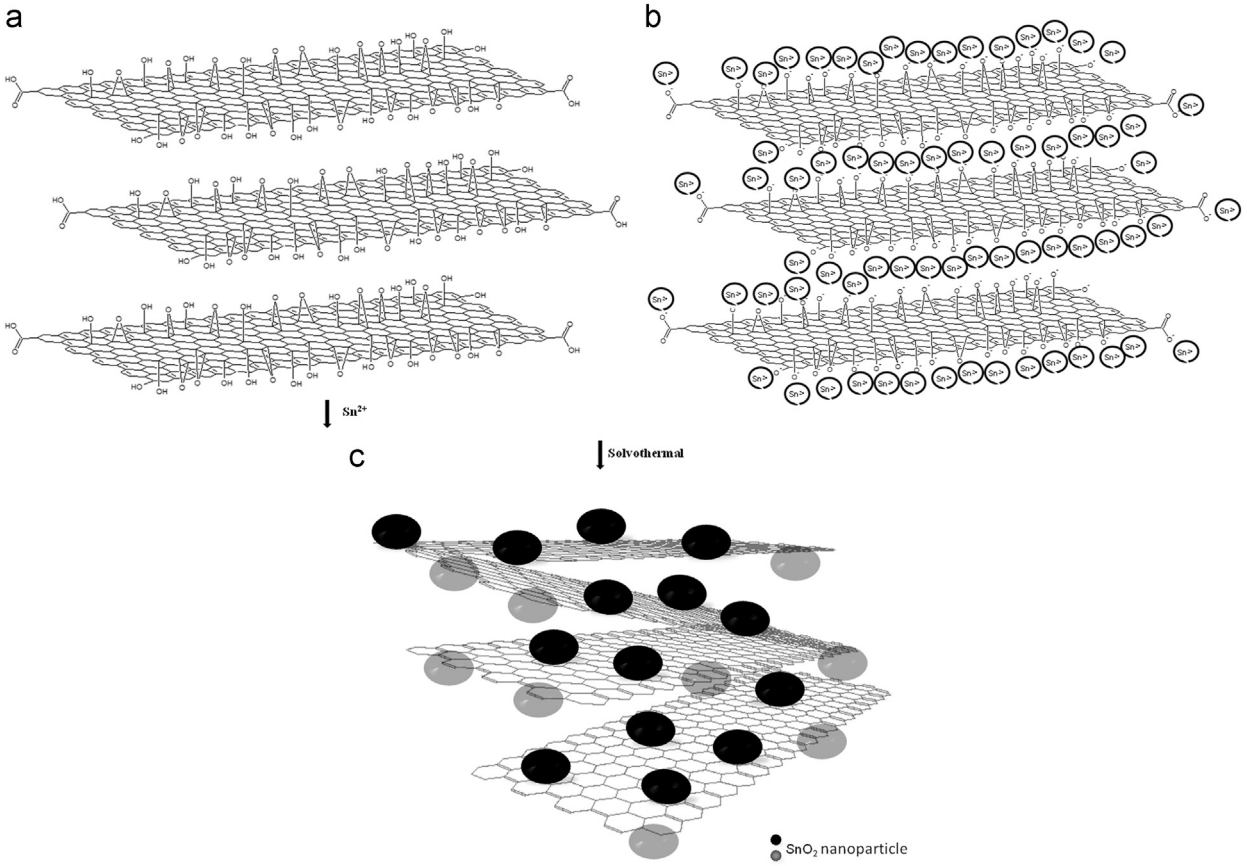

Fig. 6. Schematic formation mechanism of SnO_2/G.

correspond to the d-spacing of the (110) and (101) crystal planes of SnO_2, respectively.

The mechanism for the formation of the SnO_2/G 3D nanocomposite, illustrated in Fig. 6, can be derived from our previous work [50]. Firstly, negatively charged GO nanosheets are added to positively charged Sn^{2+} (Fig. 6a). The Sn^{2+} ions are first coordinated onto the surface of the GO nanosheets due to the electrostatic interaction between the oppositely charged ions, which are the sites for nucleation. The mobility of the large GO nanosheets that are rich in Sn^{2+} is constricted within the geometry of the autoclave, causing these nanosheets to orientate randomly, which gives rise to inevitable cross-linking among the nanosheets (Fig. 6b). The GO acts as an oxidizing agent, oxidizing Sn^{2+} to SnO_2 on the surface of GO, while GO will be simultaneously reduced to graphene. These reactions result in the growth of SnO_2 nanoparticles on the 3D graphene matrix during the solvothermal process (Fig. 6c).

The cyclic voltammetry (CV) is well known as an effective tool to investigate the capacitive behavior of a material. If the material is an ideal capacitor, it will exhibit several characteristics: high current, rectangular form of the voltammogram, and symmetry in the anodic and cathodic directions [51]. In Fig. 7(a), it can be observed that the CV curves of both SnO_2/G and graphene are nearly rectangular in shape, indicating good propagation within the electrode [52]. The specific capacitance values of the samples are calculated from the CV curves using Eq. (1) [51].

$$C_m = \frac{\int i}{m * s} \tag{1}$$

where C_m is the specific capacitance in farads per gram, $\int i$ is the integrated area of the CV curve, m is the mass of the electrode material in grams, and s is the scan rate in volts per second. According to Eq. (1), the specific capacitances of SnO_2/G and HGO are 363.3 F/g and 68.4 F/g, respectively. By inserting SnO_2 nanoparticles, the specific capacitance increased five-fold. The enhanced specific capacitance of SnO_2/G is due to the pseudocapacitance of nanosized SnO_2 decorated uniformly on the graphene surface. Based on Fig. 7(b), as the scan rate increases, the capacitance value decreases, indicating that the profiles of the two modified electrodes were gradually deformed [29].

The influence of the loading concentration of SnO_2 within the nanocomposites on the CV analysis is apparent. As shown in Fig. 7(c), the nanocomposite loaded with 5.0 mM of SnO_2 presents curves that meet the desirable criteria for a supercapacitor. Increasing the concentration of Sn^{2+} from 12.5 mM to 25 mM would decrease the

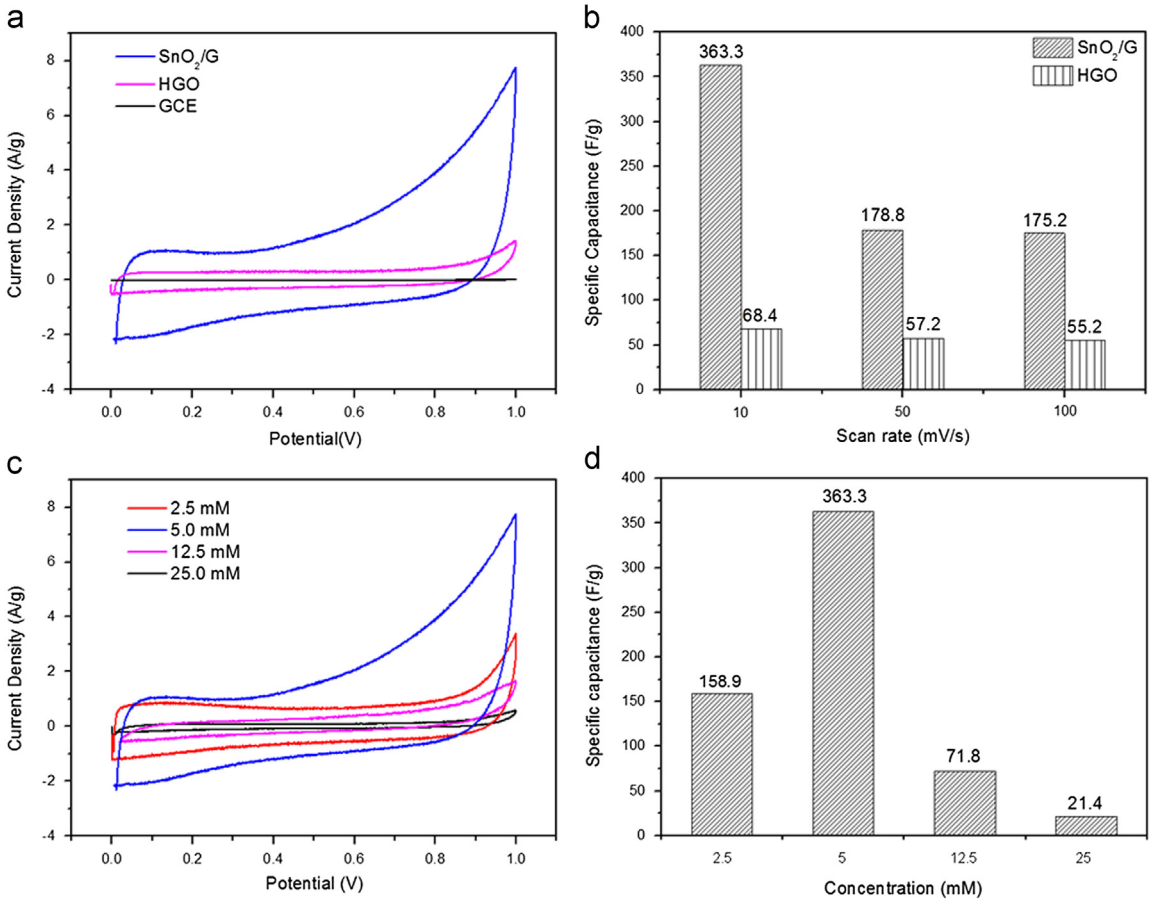

Fig. 7. (a) CVs of bare GCE, HGO and SnO_2/G in 1.0 M Na_2SO_4 at a scan rate of 10 mV/s. (b) Correlation of specific capacitance with scan rate. (c) CVs of different concentration of SnO_2 on graphene. (d) Influence of loading concentration of SnO_2 on specific capacitance of nanocomposites.

specific capacitance due to the aggregation of SnO_2 nanoparticles [29], as displayed in Fig. 7(d). A decrease in the concentration would cause the specific capacitance to decrease due to the smaller contribution of the SnO_2 nanoparticles.

The electrochemical performance was further studied using galvanostatic charge/discharge measurement, shown in Fig. 8(a). The charge/discharge curves obtained are nearly linear and symmetric, revealing a good capacitive behavior. In addition, the voltage (IR) drop is observed to be very small, which indicates that the electrodes have low internal resistance. The specific capacitance obtained for HGO and SnO_2/G from the galvanostatic charge/discharge curves are 68 and 364.3 F/g respectively. The specific capacitance value obtained for SnO_2/G is the best value thus far reported to the best of our knowledge. This is mainly due to the well decoration of SnO_2 nanoparticles on the graphene sheets, and that the SnO_2 nanoparticles acted as spacer, which leads to the increase of surface area for electrode and electrolyte accessibility.

Fig. 8(b) shows the Nyquist plot for HGO and SnO_2/G. The plots show a semicircle in the high frequency region and a straight line at low frequency region. Generally, a semicircle in the high frequency region is related to the electronic resistance within the electrode materials. Meanwhile, a vertical line that is parallel to the imaginary axis at low frequency region represents an ideal capacitive behavior. The semicircle for HGO is bigger than SnO_2/G, indicating that the polarization resistance is larger for HGO. At the low frequency region, the vertical line of SnO_2/G is almost parallel to the imaginary axis compared to that of HGO, suggesting that SnO_2/G has a better capacitive behavior than HGO. The EIS results suggest that SnO_2/G possesses a lower charge transfer resistance and better capacitive behavior compared to HGO, which is in agreement with the CV results. These characteristics is due to the synergistic effects between SnO_2 and graphene.

4. Conclusion

We successfully synthesized highly uniform SnO_2 nanoparticles with an average size of 10 nm decorated on reduced GO nanosheets via a simple and benign solvothermal method. The reduced GO hindered the agglomeration of SnO_2 nanoparticles in the hydrogel nanocomposite. Likewise, SnO_2-nanoparticle decoration prevented the graphene sheets from aggregating with one another, thus assisting in the formation of a 3D nanocomposite monolith. The CV results

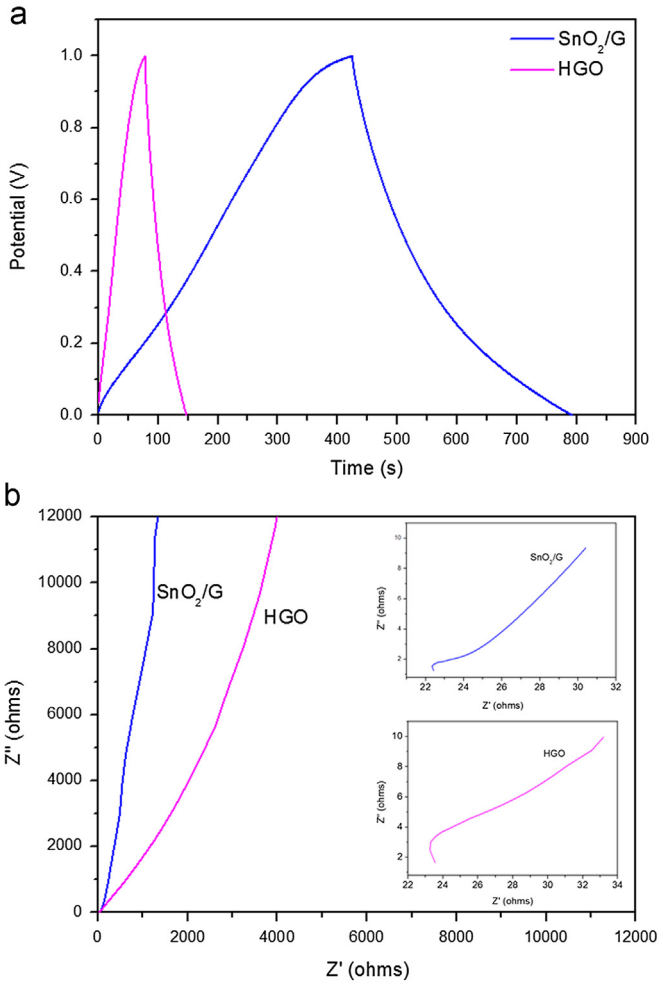

Fig. 8. (a) Galvanostatic charge/discharge curves of HGO and SnO_2/G at current density of 1.0 A/g. (b) Nyquist plots for HGO and SnO_2/G at open circuit voltage of 0 V with amplitude of 10 mV over a frequency range of 0.01 Hz to 500 kHz. Z′ = real impedance, Z″ = imaginary impedance.

indicated good capacitive behavior for SnO_2/G nanocomposites synthesized at a concentration of 5 mM of Sn^{2+}. The excellent specific capacitance of 363.3 F/g calculated from CV and 364.3 F/g calculated from charge–discharge measurement is an indication that the as-synthesized nanocomposite is a potential candidate for supercapacitor application.

Acknowledgments

This work was supported by a University of Malaya Research Grant (No. RG197/11AFR), a High Impact Research Grant of the University of Malaya (No. UM.C/625/1/HIR/030), and a High Impact Research Grant from the Ministry of Higher Education of Malaysia (No. UM.C/625/1/HIR/MOHE/05).

References

[1] L. Ran, C. Seung, B.L. Sang, Poly(3,4-ethylenedioxythiophene) nanotubes as electrode materials for a high-powered supercapacitor, Nanotechnology 19 (2008) 215710.
[2] V. Ruiz, C. Blanco, M. Granda, R. Santamaria, Enhanced life-cycle supercapacitors by thermal treatment of mesophase-derived activated carbons, Electrochimica Acta 54 (2008) 305–310.
[3] C. Portet, P.L. Taberna, P. Simon, E. Flahaut, C. Laberty-Robert, High power density electrodes for Carbon supercapacitor applications, Electrochimica Acta 50 (2005) 4174–4181.
[4] X. Hu, Z. Deng, J. Suo, Z. Pan, A high rate, high capacity and long life ($LiMn_2O_4$+AC)/$Li_4Ti_5O_{12}$ hybrid battery-supercapacitor, Journal of Power Sources 187 (2009) 635–639.
[5] J. M, B. K, Simple Capacitors to Supercapacitors - An Overview, International Journal of Electrochem. 3 (2008) 1196–1217.
[6] P. Simon, Y. Gogotsi, Materials for electrochemical capacitors, Nature Materials 7 (2008) 845–854.
[7] X. Lang, A. Hirata, T. Fujita, M. Chen, Nanoporous metal/oxide hybrid electrodes for electrochemical supercapacitors, Nature Nano 6 (2011) 232–236.
[8] Q. Li, Z. Li, L. Lin, X.Y. Wang, Y. Wang, C. Zhang, H. Wang, Facile synthesis of activated carbon/carbon nanotubes compound for supercapacitor application, Chemical Engineering Journal 156 (2010) 500–504.
[9] E. Frackowiak, F. Beguin, Carbon materials for the electrochemical storage of energy in capacitors, Carbon 39 (2001) 937–950.
[10] S.T. Mayer, R.W. Perkala, J.L. Kaschmitter, ChemInform abstract: the aerocapacitor: an electrochemical double-layer energy-storage device, ChemInform 24 (1993).
[11] M. Kaempgen, C.K. Chan, J. Ma, Y. Cui, G. Gruner, Printable thin film supercapacitors using single-walled carbon nanotubes, Nano Letters 9 (2009) 1872–1876.
[12] S.R.S. Prabaharan, R. Vimala, Z. Zainal, Nanostructured mesoporous carbon as electrodes for supercapacitors, Journal of Power Sources 161 (2006) 730–736.
[13] J. Chmiola, G. Yushin, R. Dash, Y. Gogotsi, Effect of pore size and surface area of carbide derived carbons on specific capacitance, Journal of Power Sources 158 (2006) 765–772.
[14] X. Lu, G. Wang, T. Zhai, M. Yu, J. Gan, Y. Tong, Y. Li, Hydrogenated TiO_2 nanotube arrays for supercapacitors, Nano Letters 12 (2012) 1690–1696.
[15] Z. Wu, D. Wang, W. Ren, J. Zhao, G. Zhou, F. Li, H. Cheng, Anchoring Hydrous RuO_2 on graphene sheets for high-performance electrochemical capacitors, Advanced Functional Materials 20 (2010) 3595–3602.
[16] H. Wang, J.T. Robinson, X. Li, H. Dai, Solvothermal reduction of chemically exfoliated graphene sheets, Journal of the American Chemical Society 131 (2009) 9910–9911.
[17] H. Wang, Y. Liang, T. Mirfakhrai, Z. Chen, H. Casalongue, H. Dai, Advanced asymmetrical supercapacitors based on graphene hybrid materials, Nano Research 4 (2011) 729–736.
[18] B. Zhao, J. Song, P. Liu, W. Xu, T. Fang, Z. Jiao, H. Zhang, Y. Jiang, Monolayer graphene/NiO nanosheets with two-dimension structure for supercapacitors, Journal of Materials Chemistry 21 (2011) 18792–18798.
[19] W. Zhou, J. Liu, T. Chen, K.S. Tan, X. Jia, Z. Luo, C. Cong, H. Yang, C.M. Li, T. Yu, Fabrication of Co_3O_4-reduced graphene oxide scrolls for high-performance supercapacitor electrodes, Physical Chemistry Chemical Physics 13 (2011) 14462–14465.
[20] Q. Cheng, J. Tang, J. Ma, H. Zhang, N. Shinya, L. Qin, Graphene and nanostructured MnO_2 composite electrodes for supercapacitors, Carbon 49 (2011) 2917–2925.
[21] S. Chen, J. Zhu, X. Wu, Q. Han, X. Wang, Graphene oxide-MnO_2 nanocomposites for supercapacitors, ACS Nano 4 (2010) 2822–2830.
[22] P. Si, S. Ding, X. Lou, D. Kim, An electrochemically formed three-dimensional structure of polypyrrole/graphene nanoplatelets for high-performance supercapacitors, RSC Advances 1 (2011) 1271–1278.
[23] K. Zhang, L.L. Zhang, X.S. Zhao, J. Wu, Graphene/polyaniline nanofiber composites as supercapacitor electrodes, Chemistry of Materials 22 (2010) 1392–1401.
[24] H. Wang, Q. Hao, X. Yang, L. Lu, X. Wang, A nanostructured graphene/polyaniline hybrid material for supercapacitors, Nanoscale 2 (2010) 2164–2170.

[25] Y. Wang, Z. Shi, Y. Huang, Y. Ma, C. Wang, M. Chen, Y. Chen, Supercapacitor devices based on graphene materials, Journal of Physical Chemistry C 113 (2009) 13103–13107.
[26] C. Liu, Z. Yu, D. Neff, A. Zhamu, B.Z. Jang, Graphene-based supercapacitor with an ultrahigh energy density, Nano Letters 10 (2010) 4863–4868.
[27] T.Y. Kim, H.W. Lee, M. Stoller, D.R. Dreyer, C.W. Bielawski, R.S. Ruoff, K.S. Suh, High-performance supercapacitors based on poly(ionic liquid)-modified graphene electrodes, ACS Nano 5 (2011) 436–442.
[28] M.D. Stoller, S. Park, Y. Zhu, J. An, R.S. Ruoff, Graphene-based ultracapacitors, Nano Letters 8 (2008) 3498–3502.
[29] S. Wang, S.P. Jiang, X. Wang, Microwave-assisted one-pot synthesis of metal/metal oxide nanoparticles on graphene and their electrochemical applications, Electrochimica Acta 56 (2011) 3338–3344.
[30] H. Su, T. Wang, S. Zhang, J. Song, C. Mao, H. Niu, B. Jin, J. Wu, Y. Tian, Facile synthesis of polyaniline/TiO_2/graphene oxide composite for high performance supercapacitors, Solid State Sciences 14 (2012) 677–681.
[31] S. Chen, J. Zhu, X. Wu, Q. Han, X. Wang, Graphene oxide-MnO_2 nanocomposites for supercapacitors, ACS Nano 4 (2010) 2822–2830.
[32] R.B. Rakhi, W. Chen, D. Cha, H.N. Alshareef, High performance supercapacitors using metal oxide anchored graphene nanosheet electrodes, Journal of Materials Chemistry 21 (2011) 16197–16204.
[33] X. Dong, H. Xu, X. Wang, Y. Huang, M. Chan-Park, H. Zhang, L. Wang, W. Huang, P. Chen, 3D graphene-cobalt oxide electrode for high-performance supercapacitor and enzymeless glucose detection, ACS Nano 6 (2012) 3206–3213.
[34] Z. Li, W. Shen, X. Zhang, L. Fang, X. Zu, Controllable growth of SnO_2 nanoparticles by citric acid assisted hydrothermal process, Colloids and Surfaces A: Physicochemical and Engineering Aspects 327 (2008) 17–20.
[35] S. Yang, I. Kim, M. Jeon, K. Kim, S. Moon, H. Kim, K. An, Preparation of graphite oxide and its electrochemical performance for electric double layer capacitor, Industrial and Engineering Chemistry Research 14 (2008) 365–370.
[36] S. Das, S. Chaudhuri, S. Maji, Ethanol–water mediated solvothermal synthesis of cube and pyramid shaped nanostructured tin oxide, Journal of Physical Chemistry C 112 (2008) 6213–6219.
[37] J. Ning, Q. Dai, T. Jiang, K. Men, D. Liu, N. Xiao, C. Li, D. Li, B. Liu, B. Zou, G. Zou, W.W. Yu, Facile synthesis of tin oxide nanoflowers: a potential high-capacity lithium-ion-storage material, Langmuir 25 (2009) 1818–1821.
[38] H. Wang, F. Sun, Y. Zhang, L. Li, H. Chen, Q. Wu, J.C. Yu, Photochemical growth of nanoporous SnO_2 at the air–water interface and its high photocatalytic activity, Journal of Materials Chemistry 20 (2010) 5641–5645.
[39] F. Li, J. Song, S. Gan, S. Gan, Q. Zhang, D. Han, L.N. Ari Ivaska, One-step synthesis of graphene/SnO_2 nanocomposites and its application in electrochemical supercapacitors, Nanotechnology 20 (2009) 455602.
[40] N.M. Huang, H.N. Lim, C.H. Chia, M.A. Yarmo, M. Muhamad, Simple room-temperature preparation of high-yield large-area graphene oxide, International Journal of Nanomedicine 6 (2011) 3443–3448.
[41] J.I. Paredes, S. Villar-Rodil, A. Martìl · nez-Alonso, J.M.D. Tascol · n, Graphene oxide dispersions in organic solvents, Langmuir 24 (2008) 10560–10564.
[42] M. Zhang, D. Lei, Z. Du, X. Yin, L. Chen, Q. Li, Y. Wang, T. Wang, Fast synthesis of SnO_2/graphene composites by reducing graphene oxide with stannous ions, Journal of Materials Chemistry 21 (2011) 1673–1676.
[43] O. Akhavan, Graphene nanomesh by ZnO nanorod photocatalysts, ACS Nano 4 (2010) 4174–4180.
[44] S. Stankovich, D.A. Dikin, R.D. Piner, K.A. Kohlhaas, A. Kleinhammes, Y. Jia, Y. Wu, S.T. Nguyen, R.S. Ruoff, Synthesis of graphene-based nanosheets via chemical reduction of exfoliated graphite oxide, Carbon 45 (2007) 1558–1565.
[45] A.C. Ferrari, Raman spectroscopy of graphene and graphite: disorder, electron–phonon coupling, doping and nonadiabatic effects, Solid State Communications 143 (2007) 47–57.
[46] W. Wang, C. Xu, G. Wang, Y. Liu, C. Zheng, Synthesis and Raman scattering study of rutile SnO_2 nanowires, Journal of Applied Physics 92 (2002) 2740–2742.
[47] C. Zhong, J. Wang, Z. Chen, H. Liu, SnO_2–graphene composite synthesized via an ultrafast and environmentally friendly microwave autoclave method and its use as a superior anode for lithium-ion batteries, Journal of Physical Chemistry C 115 (2011) 25115–25120.
[48] H.N. Lim, N.M. Huang, S.S. Lim, I. Harrison, C.H. Chia, Fabrication and characterization of graphene hydrogel via hydrothermal approach as a scaffold for preliminary study of cell growth, International Journal of Nanomedicine 6 (2011) 1817–1823.
[49] Y. Xu, K. Sheng, C. Li, G. Shi, Self-assembled graphene hydrogel via a one-step hydrothermal process, ACS Nano 4 (2010) 4324–4330.
[50] H.N. Lim, R. Nurzulaikha, I. Harrison, S.S. Lim, W.T. Tan, M.C. Yeo, M.A. Yarmo, N.M. Huang, Preparation and characterization of tin oxide, SnO_2 nanoparticles decorated graphene, Ceramics International 38 (2012) 4209–4216.
[51] J. Wang, Y. Xu, X. Chen, X. Du, Electrochemical supercapacitor electrode material based on poly(3,4-ethylenedioxythiophene)/polypyrrole composite, Journal of Power Sources 163 (2007) 1120–1125.
[52] Z. Xin, T.C. Bryan, B. Belen, W. Weiliang, J. Colin, S. John M, S.G. Patrick, Spray deposition of steam treated and functionalized single-walled and multi-walled carbon nanotube films for supercapacitors, Nanotechnology 20 (2009) 065605.